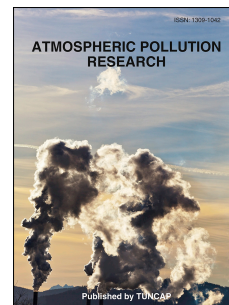


Journal Pre-proof

What the COVID-19 lockdown revealed about photochemistry and ozone production in Quito, Ecuador

María Cazorla, Edgar Herrera, Emilia Palomeque, Nicolás Saud



PII: S1309-1042(20)30256-7

DOI: <https://doi.org/10.1016/j.apr.2020.08.028>

Reference: APR 908

To appear in: *Atmospheric Pollution Research*

Received Date: 27 May 2020

Revised Date: 19 August 2020

Accepted Date: 20 August 2020

Please cite this article as: Cazorla, Marí., Herrera, E., Palomeque, E., Saud, Nicolás., What the COVID-19 lockdown revealed about photochemistry and ozone production in Quito, Ecuador, *Atmospheric Pollution Research* (2020), doi: <https://doi.org/10.1016/j.apr.2020.08.028>.

This is a PDF file of an article that has undergone enhancements after acceptance, such as the addition of a cover page and metadata, and formatting for readability, but it is not yet the definitive version of record. This version will undergo additional copyediting, typesetting and review before it is published in its final form, but we are providing this version to give early visibility of the article. Please note that, during the production process, errors may be discovered which could affect the content, and all legal disclaimers that apply to the journal pertain.

© 2020 Turkish National Committee for Air Pollution Research and Control. Production and hosting by Elsevier B.V. All rights reserved.

Author Contributions

María Cazorla: Funding acquisition, Conceptualization, Methodology, Formal analysis, Writing - Review & Editing. **Edgar Herrera:** Software, Validation, and Data Curation. **Emilia Palomeque:** Data Curation. **Nicolás Saud:** Data Curation.

What the COVID-19 lockdown revealed about photochemistry and ozone production in Quito, Ecuador

María Cazorla*, Edgar Herrera, Emilia Palomeque, Nicolás Saud

Universidad San Francisco de Quito, Instituto de Investigaciones Atmosféricas, Diego de Robles y Av. Interoceánica, Quito, Ecuador.

*mcazorla.usfq.edu.ec

Abstract

The COVID-19 lockdown presented a peculiar opportunity to study a shift in the photochemical regime of ozone production in Quito (Ecuador) before and after mobility restrictions. Primary precursors such as NO and CO dropped dramatically as early as 13 March 2020, due to school closures, but ambient ozone did not change. In this work we use a chemical box model in order to estimate regimes of ozone production before and after the lockdown. We constrain the model with observations in Quito (ozone, NO_x, CO, and meteorology) and with estimations of traffic-associated VOCs that are tightly linked to CO. To this end, we use the closest observational data of VOC/CO ratios at an urban area that shares with Quito conditions of high altitude and is located in the tropics, namely Mexico City. A shift in the chemical regime after mobility restrictions was evaluated in light of the magnitude of radical losses to nitric acid and to hydrogen peroxide. With reduced NO_x in the morning rush hour (lockdown conditions), ozone production rates at 08:30-10:30 increased from 4.2-17 to 9.7-23 ppbv h⁻¹, respectively. To test further the observed shift in chemical regime, ozone production was recalculated with post-lockdown NO_x levels, but setting VOCs to pre-lockdown conditions. This change tripled ozone production rates in the mid-morning and stayed higher throughout the day. In light of these findings, practical scenarios that present the potential for ozone accumulation in the ambient air are discussed.

Key words: ozone; ozone production; NO_x; air quality; photochemistry; COVID-19; Quito; Ecuador.

1. Introduction

The COVID-19 pandemic placed the world's public health in peril since its original outbreak in China in December 2019 (Greene, 2020). As countries across the globe implemented locking down policies and quarantined their citizens in order to combat uncontrolled infection, reductions in surface contaminants were reported in several urban areas, to the point of being observable from space (NASA, 2020; ESA, 2020). Consistently, in Quito (Ecuador) a decrease in primary pollutants (CO and NO₂) was evident as a direct result of mobility restrictions (a brief summary of events is included below), which was documented promptly in media releases (Quito Informa, 2020). However, little has been explored in regard to the effect of reduced emissions in secondary pollutants such as ozone, a highly oxidative contaminant that is health-harming of human and non-human populations (Madden and Hogswett, 2001; Ho et al., 2007). In this contribution, we analyze how mobility restrictions impacted the chemical regime of ozone production in Quito.

Quito is a city of 2.78 million inhabitants (INEC, 2017) located on the equatorial Andes, at an altitude that varies from 2400 masl (meters above sea level) in the surrounding valleys to 2800 masl at the main urban center. To place this study within the sequence of events that led to conditions of reduced emissions, a quick chronology based on official sources follows (Servicio Nacional de Gestión de Riesgos y Emergencias, 2020). The first reported case of a person infected with COVID-

19 in Ecuador occurred on 29 February 2020 in the coasts province of Guayas. As the infection began to propagate within the country, the government issued school closures at the national level on 13 March 2020. On 17 March, a decree was issued to restrict citizens' free mobility through a 21:00-05:00 national curfew. In Quito, the local government suspended public transportation (mainly composed by a fleet of diesel buses) on 17 March. The government further hardened mobility restrictions on 25 March by imposing a 14:00-05:00 curfew in the entire country. Circulation of private vehicles was limited by the last digit of their plate number. This restriction continued into April, although delivery vehicles were allowed to drive until 19:00. These measures had an impact on the levels of NO_x and VOCs and on the chemistry of ozone production, which we discuss in this paper.

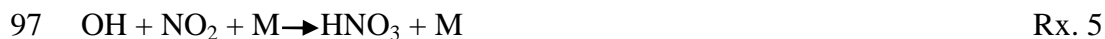
Ozone production has been studied comprehensively by many authors (i.e., Haagen-Smit et al., 1956; Finlayson-Pitts and Pitts, 1977; Thornton et al., 2002). Briefly, during daylight hours, NO_2 photolyzes and leads to the formation of ozone and NO in a 1:1 stoichiometric proportion. Subsequently, ozone is titrated by NO. The latter two reactions (summarized in Rx. 1) yield a null cycle in the clean background atmosphere. In the urban atmosphere, VOCs are oxidized by the hydroxyl radical (OH). As a result, hydroperoxy (HO_2) and organic peroxy radicals (RO_2) are formed and react with NO to produce NO_2 . These reactions produce secondary organic radicals (RO'), which continue to oxidize towards additional production of NO_2 (propagation chain compactly represented by Rx. 2 to 4). This NO_2 , that forms outside of the titration step of ozone with NO, rapidly undergoes photolysis and is converted into ozone.



Due to the above processes, the chemical rate of ozone production equals the rate of NO_2 formation from radical reactions with NO and is calculated through Eq. 1, as previously studied in several modeling and experimental work (Jaeglé et al., 2002; Shirley et al., 2006; Dusanter et al., 2009; Cazorla and Brune, 2010; Ren et al., 2013). In Eq. 1, constants k are temperature dependent rate coefficients for every reaction.

$$p(\text{O}_3) = k_{\text{HO}_2+\text{NO}}[\text{HO}_2][\text{NO}] + \sum k_{[\text{RO}_2]i+\text{NO}} [\text{RO}_2]_i [\text{NO}] \quad \text{Eq. 1}$$

Ozone production continues to be fueled in a catalytic fashion by rapid cycling of OH into HO_2 , until a termination step takes place. Termination can occur due several mechanisms of the type $\text{NO}_x\text{-HO}_x$ or $\text{HO}_x\text{-HO}_x$. Two of the most studied reactions (Sillman, 1995) are formation of nitric acid and hydrogen peroxide represented by Rx. 5 and 6, respectively (M in Rx. 5 is the altitude dependent abundance of background air molecules). The rate of radical losses due to these mechanisms can be quantified through Eq. 2 and 3 and their magnitudes can be used to assess if the ozone production regime is NO_x -saturated (Rx. 5 dominates) or NO_x -limited (Rx. 6 dominates) (Kleinman et al., 2001; Kleinman, 2005).



99
100 $L1 = k_{\text{OH}+\text{NO}_2}[\text{OH}][\text{NO}_2]$ Eq. 2

101
102 $L2 = 2k_{\text{HO}_2+\text{HO}_2}[\text{HO}_2]^2$ Eq. 3

103
104 As presented, it is necessary to count on ancillary measurements of NO_x and VOCs in order to
105 constrain chemical models for the purpose of calculating radical abundances and assessing regimes
106 of ozone production. In the present case, direct VOCs measurements are unavailable. Thus, we took
107 advantage of the fact that traffic-associated VOCs are tightly linked to ambient CO. Consequently,
108 we present VOCs derived from VOC/CO ratios taken at another high altitude Latin American city
109 (Mexico City). Furthermore, we used the dramatic change in traffic emissions during the study time
110 period as an indicator of pre- and post-lockdown precursor conditions. With these strategies, we
111 applied the Master Chemical Mechanism (MCM) (Jenkin et al., 1997; Saunders et al., 2003)
112 implemented in the Framework for 0-D Atmospheric Modeling (F0AM)(Wolfe et al., 2016) to
113 model radicals and calculate ozone production rates. The research questions we pursue in this study
114 are the following:

- 115
116 a) What are observed levels of precursors that lead to a shift in the chemical regime of ozone
117 production from NO_x -saturated to NO_x -limited in Quito?
118 b) What are practical scenarios under which high production rates could lead to accumulation of
119 ozone in the ambient air?

120
121 The organization of the paper is as follows: in the methods section, we describe the measuring site
122 as well as air quality and meteorology data sets. Furthermore, the strategy used to estimate VOCs
123 and photolysis frequencies is described in detail. In addition, we describe model details and
124 constraints. In the results section, we discuss dependencies encountered among radical abundances,
125 NO_x levels and ozone production rates, before and after the COVID-19 lockdown. We include a
126 practical view of scenarios under which increased rates of ozone production could lead to high
127 ozone days in Quito. In the conclusions section, we present the main lessons revealed by such
128 dramatic change in precursors in regard to the production of ozone and its overall effect on air
129 quality.

130 131 2. Methods

132
133 Sections 2.1 to 2.3 describe data sets and estimated quantities needed to constrain the chemical box
134 model, section 2.4 describes model settings, and sections 2.5 and 2.6 describe methodology for
135 specific analyses.

136 137 2.1. Measuring site and in situ data

138
139 Ozone, NO_x , and meteorological observations were taken at the Atmospheric Measurement Station
140 (EMA, Spanish acronym) on the main campus of Universidad San Francisco de Quito (USFQ).
141 EMA is located in the valley town of Cumbayá, east of Quito's main urban center. The station
142 coordinates are $0^\circ 11' 47''$ S, $78^\circ 26' 06''$ W, and 2414 masl. Cumbayá is an urban area that belongs to
143 the Metropolitan District of Quito. Fig. 1 shows maps with EMA's location relative to Quito and to
144 Ecuador. Additional topographic maps are presented elsewhere (Cazorla and Juncosa, 2018).

145

We present 10-minute data for NO, NO₂, and ozone from 1 January to 30 April 2020. Details relative to air quality instrumentation are described in previous work (Cazorla, 2016). Briefly, NO_x measurements were taken with a Teledyne T200 instrument. The instrument is periodically calibrated at EMA using mixtures prepared with a certified NO standard and zero air. Measurements are also intercompared against those of a neighboring City station. From calibrations, 1- σ uncertainty in measurements is 5%. The low detection limit of this instrument is 0.4 ppbv. Thus, only data greater than 0.4 ppbv were used. Ozone is continuously measured with a Thermo 49i analyzer. Ozone measurements are periodically checked by intercomparing against ground station measurements taken with conditioned electrochemical concentration cells used at EMA for vertical profiling (Cazorla, 2017). Beginning February 2020, ozone measurements are also checked periodically against a new 2B Technologies sensor model 205. The limit of detection of the 49i sensor is 0.5 ppbv. From intercomparisons, 1- σ measurement uncertainty is 8%. In addition to 10-minute time series, we present ozone, NO and NO₂ mean diurnal variations (MDV) prepared by overlapping 10-minute data each month and obtaining an average every hour.

Physical meteorology measurements (10-minute data) taken at EMA from 1 January to 30 April 2020 (temperature, pressure, relative humidity, solar radiation, and precipitation) are also presented. Details of the meteorological context within which this work was developed are included in the Supplementary Material (SM), Appendix S1 (Table S1, Fig. S1.1 and S1.2). Briefly, average temperature maximum from January to April was 23-24°C, while the relative humidity at noon was 40-50%. January was the month with the greatest number of sunny days (from the 7th to the 19th) and no rain (19 days). On the other hand, April was the cloudiest month during which there were rain events at different hours in 20 days. Total precipitation in January, February, March, and April was 74.9, 112.9, 99.8, and 145 mm, respectively. In general, at the measuring site, cooler temperatures, more cloudiness, and rain are typical from February to May and around November, while the summer months run from July to mid-September (Cazorla and Juncosa, 2018). Information about meteorological instrumentation at EMA can be found elsewhere (Cazorla and Tamayo, 2014). Instruments were calibrated against independent standards from which uncertainty in meteorological data is 5%.

Carbon monoxide measurements are unavailable at EMA. Thus, CO data were obtained as 1-hour averages from Quito's air quality network and public archive (Secretaría de Ambiente, 2020). The car fleet and the traffic situation during weekday rush hours are comparable in the entire Metropolitan District for which we worked under the assumption that CO levels are similar, on average, within the urban area. Thus, we chose three stations within the city (stations marked in Fig. 1, coordinates and details in the SM, Appendix S2, Fig. S2) and obtained an average CO time series for the study time period. Mean diurnal variations before and after the lockdown are presented in the results section. The standard deviation among the three sample stations was used as a measure of uncertainty for CO, which corresponds to +/-26% at the 1- σ level. Stations were chosen based on data quality and completeness. To constrain the model, CO data was linearly interpolated to match EMA's 10-minute time stamp.

2.2 Derivation of VOCs

Direct VOCs observations are unavailable in Quito. Thus, traffic-borne VOCs, which are intimately linked to CO (Bon et al., 2011), were derived using VOC/CO ratios from a similar urban area. Hence, we used measurements of non-methane VOCs as well as CO by Jaimes-Palomera et al. (2016) in the Mexico City Metropolitan Area from March to May 2012. Mexico City, located at 2550 masl in the tropics, shares with Quito conditions of high altitude that directly influences combustion and levels of VOCs as previous work demonstrates (Nagpure et al., 2011; Fang et al.,

2019). Hence, Mexico City's measurements are the closest observational data suitable to be applied in the present case. To be precise, the work published by Jaimes-Palomera et. al. presents average diurnal profiles of VOCs and CO that represent typical urban conditions. Thus, we correlated VOCs with CO to obtain VOC/CO ratios for: propane, 3-methylpentane, n-butane, n-hexane, ethene, propene, benzene, toluene, m-xylene, and ethylbenzene. Ratios range from 0.0062 (3-methylpentane) to 0.06 (propane). All factors and data are presented in the SM (Appendix S3, Table S3). Subsequently, we used Quito CO observations to derive VOCs and constrain the chemical box model, as discussed in section 2.4.

2.3. Estimations of NO₂ and ozone frequencies of photolysis

Photolysis frequencies of NO₂ (J_{NO_2}), used to constrain the photochemical box model, were estimated following Trebs et al. (2009). Thus, we used 10-minute station measurements of global solar radiation (Fig. S1.1) taken at EMA. However, this empirical model was proposed for sites at altitudes lower than 800 masl. Due to this caveat, an alternative estimation was performed using measurements taken in Mexico City in March 2006. This comparison is suitable for observations were performed in a city in the tropics and at high altitude. Hence, J_{NO_2} measurements in Mexico City documented by Li et al. (2011) were correlated to solar radiation measurements taken by Fast et al. (2007) and a simple scaling factor was obtained from a linear regression (details in the SM, Appendix S4, Fig. S4). This factor was applied to the solar radiation time series taken at EMA in order to estimate J_{NO_2} . These calculations yielded upper and lower limits for J_{NO_2} (Trebs' method and Mexico City measurements, respectively). Hence, we present the average of both methods as J_{NO_2} estimates and use the difference between the boundaries as a measure of 1- σ uncertainty (+/- 17% at noon and +/- 32% in the mid-morning and afternoon). Subsequently, a simple scaling factor of 4.67×10^{-3} (obtained from simple observation) that relates J_{NO_2} to $J_{O_3 \rightarrow O_1D}$ was extracted from the work by Li et al. (2011). We applied this factor to Quito's J_{NO_2} to find ozone frequencies of photolysis. Both, J_{NO_2} and $J_{O_3 \rightarrow O_1D}$, were used to constrain the chemical box model. Additional frequencies of photolysis for other atmospheric species were calculated by the model, as explained in the following section.

2.4 Model details

We used the Framework for 0-D Atmospheric Modeling (Wolfe, 2016), F0AM v4, which is a complete MATLAB-based software loaded with six ready-to-use atmospheric chemistry mechanisms as well as with three options for resolving photolysis frequencies. The F0AM has been extensively used and proven to be a powerful tool for photochemical simulations (i.e., Brune et al., 2019). In the present case, we used the Master Chemical Mechanism (Jenkin et al., 1997; Saunders et al., 2003), MCM v3.3.1, obtained via website (<http://mcm.leeds.ac.uk/MCM>). Thus, a subset of reactions for the 10 VOCs indicated previously were prepared directly from the MCM website and added as code to the F0AM. The chosen photolysis option in the F0AM was the MCM parametrization (Wolfe, 2016). The model was constrained using measurements of ozone, NO, NO₂, CO, meteorological data, ten non-methane hydrocarbons (section 2.2), J_{NO_2} and $J_{O_3 \rightarrow O_1D}$ (section 2.3). The code was set to correct all modeled photolysis frequencies according to the J_{NO_2} structure in order to account for the effect of clouds.

The model was run from 1 January to 30 April 2020 in 10-minute time steps. Model runs were performed at EMA in a system that has a Core i7 processor with 32 GB of RAM memory and a MATLAB license owned by USFQ. The following quantities from the model output were used in analyses: radical abundance (OH, HO₂, and RO₂), concentrations of secondary species

(formaldehyde and HONO), corresponding reaction coefficients, and frequencies of photolysis. A complete description of model output can be found elsewhere (Wolfe, 2020).

2.5 Radical and ozone production rates

The chemical production of HO_x radicals, p(HO_x), was obtained considering the main mechanisms for the production of OH and HO₂, namely ozone photolysis followed by reaction of O(¹D) with water vapor (Levy, 1971), HONO photolysis, and formaldehyde photolysis (Dusanter et al., 2009; Ren et al, 2013). To this end, we used measurements of ozone and water vapor as well as model output concentrations of HONO, formaldehyde, and their photolysis frequencies. Consequently, Eq. 4 was used to calculate p(HO_x), as in previous work (Thornton et al, 2002; Ren et al., 2013).

$$p(\text{HO}_x) = 2J_{\text{O}_3 \rightarrow \text{O}(1\text{D})}[\text{O}_3][k_{\text{O}(1\text{D})+\text{H}_2\text{O}}[\text{H}_2\text{O}]/(k_{\text{O}(1\text{D})+\text{H}_2\text{O}}[\text{H}_2\text{O}] + k_{\text{O}(1\text{D})+\text{M}}[\text{M}])] + 2J_{\text{HCHO}}[\text{HCHO}] + J_{\text{HONO}}[\text{HONO}] \quad \text{Eq. 4}$$

Ozone production rates were calculated using Eq. 1. To this end, we used model output radical abundances (HO₂ and RO₂) and rate coefficients as well as station measurements of NO. For comparisons, we filtered data within similar ranges of J_{NO_2} as cloudiness and precipitation substantially increased from January to April. A discussion is included in the results section.

Ozone production regimes were evaluated by looking into the magnitude of precursor losses to nitric acid (L1, Eq. 2) and hydrogen peroxide (L2, Eq. 3). Thus, the ratio L1/(L1+L2) was evaluated and discussed in light of previous work (Kleinman et al., 2001; Ren et al., 2013).

2.6. Test simulation with reduced NO_x

Ozone production rates, calculated with the above procedure, were also determined for the hypothetical case that NO_x levels stayed low, while CO and VOCs were those of normal pre-lockdown conditions. This estimation was done to discuss more extensively potential scenarios that could lead to a more permanent shift in the chemical regime of ozone production in Quito. This test was done with NO_x, ozone, and meteorological data from 14 March to April, but mimicking CO and VOCs levels from before the quarantine. Thus, the CO and VOCs levels from 14 March to April were multiplied by a factor of 1.86 to perform this simulation. A discussion is included in the results section.

3. Results and discussion

3.1 Air quality observations

Under typical conditions, the study area is characterized by intense traffic, mainly during weekdays and in months when school and college classes are active. At USFQ, the spring semester runs from the second week of January to early May, while classes in the national school system (for provinces in the Ecuadorian highlands) extend up to July. Thus, rush hour emissions from private vehicles and public transportation, that become well mixed in the boundary layer, are evident in air quality measurements. NO and NO₂ observations taken at EMA USFQ before and after the lockdown are presented in Fig. 2a and b (the SM, Appendix S5, Fig. S5 contains time series).

As presented, morning rush hour levels of NO approach 100 ppbv (10-minute data). The local legislation does not impose NO_x emission controls on vehicle exhausts, which explains rush hour NO levels of the magnitudes depicted in Fig. 2. In addition, boundary layer depths during morning

rush hours are shallow (below 500 m from 07:00-09:00), as calculated from station measurements (Cazorla and Juncosa, 2018) (SM, Appendix S6, Fig. S6). This physical factor contributes to concentrating primary emissions near the ground in the morning. Under quarantine conditions, NO_x maxima plummeted by a factor of five from mid-March into April. In mid-March the reduction was greater, but in April permits were implemented for delivery vehicles and medical emergencies, which somewhat increased the traffic flow.

In regard to carbon monoxide (Fig. 3), average changes after the initiation of the lockdown period are evident as levels dropped by a factor of 1.86 (from about 973 to 523.5 ppbv in the morning rush hour). It is important to remark that CO was not measured at EMA station, which is a limitation. However, CO levels are similar across different stations managed by the local network as presented in their annual reports (Secretaría de Ambiente, 2018). Therefore, it is reasonable to assume that an average within Quito yields a good estimate of mean CO levels before and after the COVID-19 lockdown. Figure 3 also contains average levels (before and after the lockdown) of propene, one of the ten VOCs derived from VOC/CO ratios. Previous work demonstrates the high correlation of traffic-related VOCs with CO, in particular at high altitude, where elevation plays a role at increasing VOCs emissions (Bon et al., 2011; Nagpure et al., 2011; Fang et al., 2019). Hence, estimating VOCs levels with observed factors from another high elevation Latin American city is suitable for the present case. In addition, pandemic-induced mobility restrictions marked a clear difference between levels of traffic-related compounds that also make reasonable scaling VOCs to CO. Consequently, Fig. 3 shows that propene dropped proportionally along with CO. The SM (Fig S3) contains data of all VOCs derived for this work.

While primary precursors decreased considerably after 13 March, the day school closures were issued, and stayed low into April, ozone levels did not experience evident changes. Fig. 4 shows that 10-minute maxima peaked at 45-50 ppbv from January to April 2020. From diurnal variations, average peak ozone before and after 13 March was about 33 ppbv. Daily data (SM, Appendix 7, Fig. S7.1) shows that noontime maxima in January were lower, on average, than levels in February and March, even though it was the sunniest month of the trimester. Also, titration with NO at around 06:00 (local time) was reduced during the quarantine due to reduced morning rush hour NO. A more dramatic comparison is average ozone in January and April, which are comparable (SM, Fig. S7.2), even though April was considerably more cloudy and had more precipitation. Thus, questions arise in regard to levels of ozone from January to April in connection with the drastic reduction in emission precursors after 13 March. An explanation based on photochemistry follows.

3.2 Meteorological influence on photolysis

Photolysis reactions in the atmosphere directly depend on the amount of solar radiation available for the dissociation of molecules (Seinfeld and Pandis, 2006). In particular, ozone formation is highly sensitive to NO₂ photolysis. Likewise, HO_x radicals are formed due to photolysis of ozone and other important species in the urban atmosphere, such as HONO and formaldehyde. In the present case, the pandemic lockdown took place during months that seasonally transitioned from sunny skies in January into more cloudy conditions with increased precipitation in April. This changing meteorological conditions resulted in variability of J_{NO_2} diurnal profiles across the months, before and after the lockdown, as depicted in Fig. 5a. Thus, before the quarantine, January was consistently sunny, which led to J_{NO_2} maxima at noon, while the first half of March had sunny mornings but cloudy afternoons. The second half of March was comparable to February in terms of noontime J_{NO_2} , but April was mostly cloudy. In order to compare photochemical quantities before and after the lockdown in a way that the effect of precursors can be assessed, while keeping physical factors constant, we used data that corresponds to sunny conditions in the entire time series (the complete

data set was treated equally, details of data filtering in the SM, Appendix 8, Fig. S8). Hence, mean J_{NO_2} profiles from January to 13 March and from 14 March to April, that correspond to sunny conditions, are presented in Fig. 5b. Therefore, radical abundance and ozone production rates are discussed in terms of equal conditions of J_{NO_2} .

3.3 Radical abundance and production

Average OH radical abundance under sunny conditions in the periods before and after the COVID-19 lockdown are depicted as diurnal profiles in Fig. 6a. Under post-lockdown conditions (14 March to April), OH radicals began to rise as early as 07h30 and remained higher than under regular traffic conditions throughout the day. In the morning, between 08:30-11:30, OH ranged from 0.07-0.55 pptv before 14 March, while afterwards it rose to 0.23-0.68 pptv. This feature is not due to physical reasons because solar radiation conditions are kept identical. Hence, additional radical abundance is due to atmospheric chemistry as the chemical depletion of radicals due to high NO_x levels decreased during the lockdown, in particular in the morning rush hour (this feature is explained further below with magnitudes of radical loss). Likewise, the abundance of hydroperoxy and organic peroxy radicals (HO_2 and RO_2) increased (Fig. 6b and c) during the lockdown from a sum of 24 to 39 pptv at noon, on average. As in the previous case, this is a chemical effect of OH reacting with VOCs under reduced NO_x conditions as opposed to radicals being depleted by large amounts of NO_x (Seinfeld and Pandis, 2006; Ren et al., 2013). Furthermore, cycling between HO_2 and OH was faster during the lockdown throughout the day as given by HO_2/OH ratios in Fig. 7a. The test simulation with pre-lockdown levels of VOCs and post-lockdown (reduced) levels of NO_x shows that in the absence of elevated NO_x , OH is comparable to observed post-lockdown conditions, but at midday cycling between HO_2 and OH has the potential to almost triple with regard to regular traffic conditions (Fig. 7a). For this reason, in the test simulation noontime abundance of OH is lower, but HO_2 and RO_2 abundances are substantially higher.

Radicals presented in Fig. 6 come from the main known sources of OH and HO_2 in the urban atmosphere: ozone photolysis followed by reaction of $O(^1D)$ with water vapor as well as formaldehyde and HONO photolysis (Dusanter et al., 2009; Ren et al., 2013). The first source was calculated with the first term of Eq. 4 and is depicted with a blue line in all panels in Fig. 8. Water vapor, ozone, and solar radiation were similar before and after the lockdown for which this source of OH radicals was about constant with peak values of 0.4-0.45 pptv s^{-1} for the study time period (including the reduced- NO_x test) (Fig. 8a to c).

Formaldehyde photolysis is a major source of hydroperoxy radicals in the urban atmosphere (complete reactions can be found in Seinfeld and Pandis, 2006). Formaldehyde is formed along the oxidation chain, when VOCs react with OH. In the present case, we used the formaldehyde model output (SM, Appendix 9, Fig. S9) and its corresponding model J_{HCHO} in order to calculate this contribution to $p(HO_x)$ (second term of Eq. 4, depicted by the red dotted line in all panels in Fig. 8). During the study time period, formaldehyde photolysis was more important after the lockdown, mainly in the morning. Thus, magnitudes were 1.8 and 1.6 times higher at 09:00 and 10:00, respectively (the SM, Appendix 10, Fig S10 shows curves in Fig. 8 overlapped by contribution). At noon, this source of radicals was about 0.3 pptv s^{-1} throughout the study time period as NO before the lockdown decreased after the morning rush hour, while during the lockdown stayed low (Fig. 2). The test simulation with pre-lockdown levels of VOCs, but reduced (post-lockdown) levels of NO_x (Fig. 8c) further backs this chemical result as the photolysis of formaldehyde became as important as ozone photolysis in regard to producing HO_x radicals. These results are consistent with previous work that shows how in urban environments (for example in Mexico City) the contribution of formaldehyde photolysis accounts for up to 40% of HO_x radicals (Shirley et al., 2006). In the

present case, we estimate that this source contributes with about 34% to the total radical production rate.

HONO photolysis is also a significant source of radicals, mainly in the morning during the traffic rush hour, as demonstrated by former studies (Dusanter et al. 2009; Ren et al., 2013). As in the previous case, this contribution was calculated with the third term of Eq. 4 and using the MCM model output for HONO (SM, Fig. S9) and J_{HONO} . This contribution was 1.4 times higher before the lockdown as rush-hour NO_x was five times higher. The test done with reduced levels of NO_x is consistent, as this contribution was comparable to post-lockdown conditions.

In this study we rely in the robustness of observation-based methods to find estimates of radical production rates from the first source (O^1D+H_2O), while the other two sources come from modeling. Hence, from propagation of error, we estimate that uncertainty ($1-\sigma$) in the first source is 32% (considering uncertainties in $J_{O3 \rightarrow O1D}$ as well as in ozone and water vapor measurements reported in the methods section). For radical production due to formaldehyde and HONO photolysis (as well as for radical abundance), at the moment we assume model uncertainty reported in the literature (i.e., Brune et al., 2019) of 35%. Likewise, we estimate that uncertainty in other photochemical quantities (radical abundance and ozone production) is similar, but in the future these estimations need to be re-checked as measurements of physical and chemical quantities become available in the study area.

3.4 Ozone production rates and regimes

The mean diurnal variation of ozone production rates before and after the lockdown are depicted in Fig. 7b. During the quarantine, ozone production rates at 08:30-10:30 increased from previous 4.2-17 to 9.7-23 ppbv h^{-1} . These results are consistent with the former section in the sense that under regular traffic conditions high morning NO_x levels constrain ozone production due to a lack of sufficient radicals to react with NO and produce ozone. Quarantine conditions induced a chemical shift that led to increased availability of HO_2 and RO_2 radicals that combined with reduced morning NO_x led to higher ozone production rates. Radical abundance being at the core of the observed shift in regimes of ozone production can be assessed by looking into the magnitude of paths for radical losses to nitric acid (L1) and to hydrogen peroxide (L2). Fig. 9 depicts the ratio of L1 to the total loss $L1+L2$. When the radical loss to hydrogen peroxide is as important as the radical loss to nitric acid, the ratio becomes 0.5. A ratio much greater than 0.5 has been shown to indicate a VOC-limited (NO_x -saturated) regime (Kleinman et al., 2001; Kleinman, 2005; Ren et. al., 2013). As presented, L2 was more significant under quarantine conditions, while this term had little effect from January to 13 March. Consequently, the time period from January to the first half of March was strongly NO_x -saturated. In contrast, after 13 March, losses to hydrogen peroxide were of increasing importance, which confirms a shift in the chemical regime of ozone production. The test calculation done with reduced NO_x at post-lockdown levels, but mimicking pre-lockdown VOCs, pushed even further this shift towards the NO_x -limited zone as ozone production tripled in the mid-morning (Fig. 7b) and stayed high, while $L1/(L1+L2)$ became even lower (Fig. 9). The SM (Appendix 11, Fig. S11) shows individual magnitudes of L1 and L2 for all cases.

The dependence of $p(O_3)$ with NO, before and after the lockdown, as well as for the reduced NO_x scenario, is depicted in Fig. 10 with indication of $p(HO_x)$ magnitudes. As presented, under regular conditions ozone production is strongly suppressed under a NO_x -saturated regime (Fig. 10a). In this regime, $p(O_3)$ decreases with increasing NO, whose levels approach 100 ppbv. After 13 March (Fig. 10b), the drop in NO emissions augmented the rate of ozone production, which steadily grows at low NO and at the higher $p(HO_x)$ range, and then decreases as NO continues to increase. With

reduced NO, but “normal” VOCs, this same dependence occurs (Fig. 10c), although at higher magnitudes of $p(\text{O}_3)$ that reached values higher than 40 ppbv h^{-1} (10-minute data). In all cases, $p(\text{O}_3)$ is higher at higher levels of $p(\text{HO}_x)$ and at the low NO boundary. A transition in the regime occurs at 2-3 ppbv of NO, when $p(\text{O}_3)$ decreases (describing a curve) with increasing NO (Fig. 10b and c). This final analysis is consistent with seminal work on ozone production (Thornton et. al., 2012) that demonstrates the high non-linearity of ozone production rates with NO when data is sorted by $p(\text{HO}_x)$ levels.

3.5 Final remarks

In spite of limitations and uncertainties, the above results point towards relevant aspects in regard to photochemical regimes of ozone production in Quito in connection to air quality. First, ozone production rates under typical conditions of intense traffic and solar radiation are constrained by high NO_x levels. For example, 10-18 January was a warm and sunny time period with abundant traffic emissions, but ozone levels were the lowest of the trimester (maxima at about 30 ppbv, SM, Fig. S7.1). Ambient ozone is the result of several contributions in a mass balance, namely chemical production and loss, dry and wet deposition, and horizontal advection. Although further modeling is needed to unveil the contribution of advection, observations indicate that average ozone production rates reported in this work, under the meteorological conditions from January to mid-March, do not lead to ambient ozone accumulation. Furthermore, the presence of traffic emissions poses the question of the chemical fate of precursors in Quito's ambient air. Future work needs to focus on quantifying other fractions of photochemical smog such as peroxyacetyl nitrate (PAN), nitric acid, and nitrate particles in Quito.

A second important lesson is that a reversal in emission precursors in Quito is capable of shifting the chemical regime to the NO_x -limited zone, which results in higher ozone production rates. Quarantine conditions, a current reality and one that could repeat itself in the near future, supply higher ozone production rates. Average morning magnitudes, that doubled those before the quarantine, were capable of sustaining the same levels of ozone in Quito, even in months that are seasonally cloudier and with more abundant precipitation. Thus, meteorological conditions played a role in the ozone mass balance providing less sunny days and cleaning the atmosphere through wet deposition. However, if confinement orders took effect in the hot and dry summer months of August and September, higher ozone production rates at low NO_x levels could contribute to the accumulation of ozone in the boundary layer, in particular under conditions of stagnant air. This is a realistic scenario that needs to be watched closely under the current reality of a pandemic that poses the need of periodical quarantines to control the spread of the disease.

Thirdly, results obtained from calculations with reversed levels of precursors shed light to investigating the chemical reasons that underlie few observed episodes of high ozone in Quito. These events have been associated to wildfires (for example on 1 October 2018), as it was recently presented in a preliminary study (Cadena et al., 2019). However, the true chemical nature of such events needs yet to be scrutinized through studies that involve measurements and modeling. Although the complex effect of advection of air masses from biomass burning regions is beyond the scope of this work, it is important to document that the current study advances the topic of potential scenarios that cause a shift in the chemical regime of ozone production due to drastic changes in the proportion of organic compounds with respect to NO_x .

Finally, a situation that could potentially cause increased ozone is the hypothetical case that NO_x emission controls in vehicles were to be imposed. Such scenario would cause a shift of the sort mimicked by the reduced- NO_x calculation, in which normal levels of organic compounds combined

with permanently low NO_x lead to higher ozone production rates. This scenario emphasizes on the fact that environmental practices, that have to do with emission controls, need to carefully take into account that the regime of ozone production depends on the local makeup of pollutants in the ambient air and is non-linear with respect to precursor levels.

Even though intensive work that incorporates measurement campaigns to constrain chemical and transport models still needs to be developed, the present contribution points out for the first time to specific conditions and identifies practical scenarios under which the chemical regime shifts towards higher rates of ozone production.

4. Conclusions

The COVID-19 mobility restrictions and lockdown, that initiated with school closures on 13 March in Quito (Ecuador), marked a shift in primary emissions that was used to reveal the chemical nature of ozone production under regular conditions as well as under reduced levels of precursors. First, low ozone production rates, in spite of abundant urban emissions and equatorial solar radiation, are the rule as radicals are quickly depleted by loss mechanisms of the type $\text{NO}_x\text{-HO}_x$. Results indicate that, under normal traffic conditions, radical loss to nitric acid dominates, in particular in the morning rush hour, when NO spikes (10-minute data) approach 100 ppbv. In contrast, post-lockdown NO_x levels decreased by a factor of five during daytime. This shift led to less radical losses to nitric acid, while the loss to hydrogen peroxide became increasingly important. Thus, the abundance of HO_2 and RO_2 increased from a total of 4.2 pptv in the mid-morning before the lockdown to 16.1 pptv during the quarantine, while at noon it increased from previous 23.6 to 39 pptv. Consistently, OH in the morning at 08:30-10:30 increased from 0.07-0.37 pptv before the lockdown to 0.23-0.61 pptv afterwards, while $\text{p}(\text{O}_3)$ increased from 4.2-17 to 9.7-23 ppbv h^{-1} , respectively. From observations, magnitudes of pre-lockdown ozone production rates factored with dilution within the boundary layer and advection explain generally low ambient ozone in Quito, but further work needs to be developed to better understand transport effects. As per ozone production during the lockdown, there was seasonally more cloudiness and precipitation during mid-March and April, which helped clean the atmosphere through wet deposition. Hence, meteorological conditions were favorable at preventing ozone accumulation during this period. However, if a quarantine were to take effect during the warmer summer months of August to mid-September, especially if conditions of stagnant air and temporary drought develop, increased rates of ozone production would pose a threat of accumulation in the ambient air. To test further the effect of a shift in emissions that could lead to even higher ozone production rates, a simulation with post-lockdown NO_x levels, but pre-lockdown VOCs and sunny conditions yielded a total of 52 pptv of HO_2 and RO_2 at noon and $\text{p}(\text{O}_3)$ of 33 ppbv h^{-1} , on average (higher than 40 ppbv h^{-1} as 10-minute data). A scenario that would cause a permanent shift towards this regime would be if NO_x emission controls on vehicle exhausts, currently not applied, were to be enforced. Although such scenario is not a current risk, from a scientific and academic standpoint it is prudent to remark that such situation would have an impact on air quality as it would cause a shift in the chemical regime towards producing ozone at higher rates. In spite of many limitations, the change in emissions due to the COVID-19 lockdown was substantial enough to reveal critical information in regard of precursor levels that cause a shift in the regime of ozone production. This contribution advances our understanding of the underlying chemistry of photochemical smog in Quito, Ecuador.

Author Contributions

María Cazorla: Funding acquisition, Conceptualization, Methodology, Formal analysis, Writing - Review & Editing. **Edgar Herrera:** Software, Validation, and Data Curation. **Emilia Palomeque:** Data Curation. **Nicolás Saud:** Data Curation.

Declaration of competing interest

Authors declare not to have conflict of interest.

Acknowledgements

This study was funded by USFQ PoliGrant 2020. Sponsorship of the Vienna Convention Trust Fund, through agreement No. 224581 with the World Meteorological Organization, considerably augmented ozone research capacity at EMA USFQ. We thank Secretaría de Ambiente de Quito for making available air quality data in the public archive.

References

- Bon, D.M., Ulbrich, I.M., de Gouw, J.A., Warneke, C., Kuster, W.C., Alexander, M.L., Baker, A., Beyersdorf, A.J., Blake, D., Fall, R., Jimenez, J.L., Herndon, S.C., Huey, L.G., Knighton, W.B., Ortega, J., Springston, S., Vargas, O. 2011. Measurements of volatile organic compounds at a suburban ground site (T1) in Mexico City during the MILAGRO 2006 campaign: measurement comparison, emission ratios, and source attribution. *Atmos. Chem. Phys.*, 11, 2399–2421, <https://doi.org/10.5194/acp-11-2399-2011>
- Brune, W.H., Miller, D.O., Thames, A.B., Allen, H.M., Apel, E.C., Blake, D.R., Bui, T.P., Commane, R., Crounse, J.D., Daube, B.C., Diskin, G.S., DiGangi, J.P., Elkins, J.W., Hall, S.R., Hanisco, T.F., Hannun, R.A., Hints, E.J., Hornbrook, R.S., Kim, M.J., McKain, K., Moore, F.L., Neuman, J.A., Nicely, J.M., Peischl, J., Ryerson, T.B., St. Clair, J.M., Sweeney, C., Teng, A.P., Thompson, C., Ullmann, K., Veres, P.R., Wennberg, P.O., Wolfe, G.M. 2019. Exploring Oxidation in the Remote Free Troposphere: Insights From Atmospheric Tomography (ATom). *J. Geophys. Res. - Atmos.*, 125(1). <https://doi.org/10.1029/2019JD031685>.
- Cadena, E., Daza, J., Cazorla, M. 2019. Congreso Anual de Meteorología y Calidad del Aire (CAMCA). Eventos de ozono alto en Quito y sus precursores. Quito: Instituto de Investigaciones Atmosféricas IIA USFQ. URL https://www.usfq.edu.ec/eventos/camca/Documents/LibroAbstracts_CAMCA2019.pdf. Accessed date: 25 May 2020.
- Cazorla, M., Brune, W.H. 2010. Measurement of Ozone Production Sensor. *Atmos. Meas. Tech.*, 3, 545–555. <https://doi.org/10.5194/amt-3-545-2010>.
- Cazorla, M., Tamayo, E. 2014. Atmospheric measurement station at Universidad San Francisco de Quito (EMA): ground-based physical meteorology instrumentation and assessment of initial measurements. *Av. Cienc. Ing. (Quito)* 6(2), C21–C30. <https://doi.org/10.18272/aci.v6i2.184>.
- Cazorla, M. 2016. Air quality over a populated Andean region: Insights from measurements of ozone, NO, and boundary layer depths. *Atmos. Pollut. Res.*, 7(1), 66–74. <https://doi.org/10.1016/j.apr.2015.07.006>

- 593
 594 Cazorla, M. 2017. Ozone structure over the equatorial Andes from balloon-borne observations and
 595 zonal connection with two tropical sea level sites. *J. Atmos. Chem.*, 74, 377–398.
 596 <https://doi.org/10.1007/s10874-016-9348-2>
 597
- 598 Cazorla, M., Juncosa, J. 2018. Planetary boundary layer evolution over an equatorial Andean valley:
 599 A simplified model based on balloon-borne and surface measurements. *Atmos. Sci. Lett.*, 19(8),
 600 e829. <https://doi.org/10.1002/asl.829>
 601
- 602 Dusanter, S., Vimal, D., Stevens, P. S., Volkamer, R., Molina, L. T., Baker, A., Meinardi, S., Blake,
 603 D., Sheehy, P., Merten, A., Zhang, R., Zheng, J., Fortner, E. C., Junkermann, W., Dubey, M., Rahn,
 604 T., Eichinger, B., Lewandowski, P., Prueger, J., Holder, H., 2009. Measurements of OH and HO₂
 605 concentrations during the MCMA-2006 field campaign – Part 2: Model comparison and radical
 606 budget. *Atmos. Chem. Phys.* 9, 6655–6675. <https://doi.org/10.5194/acp-9-6655-2009>.
 607
- 608 ESA. 2020. Coronavirus lockdown leading to drop in pollution across Europe. URL
 609 [https://www.esa.int/Applications/Observing_the_Earth/Copernicus/Sentinel-](https://www.esa.int/Applications/Observing_the_Earth/Copernicus/Sentinel-5P/Coronavirus_lockdown_leading_to_drop_in_pollution_across_Europe)
 610 [5P/Coronavirus_lockdown_leading_to_drop_in_pollution_across_Europe](https://www.esa.int/Applications/Observing_the_Earth/Copernicus/Sentinel-5P/Coronavirus_lockdown_leading_to_drop_in_pollution_across_Europe). Accessed date: 25 May
 611 2020.
 612
- 613 Fang, L., Lou, D., Hu, Z., Tan, P. 2019. The Emission Characteristics of a Diesel Engine During
 614 Start-Up Process at Different Altitudes. *Energies*, 12(18), 3556.
 615 <https://doi.org/doi:10.3390/en12183556>
 616
- 617 Fast, J.D., de Foy, B., Acevedo Rosas, F., Caetano, E., Carmichael, G., Emmons, L., McKenna, D.,
 618 Mena, M., Skamarock, W., Tie, X., Coulter, R.L., Barnard, J.C., Wiedinmyer, C., and Madronich,
 619 S., 2007. A meteorological overview of the MILAGRO field campaigns. *Atmos. Chem. Phys.* 7,
 620 2233–2257. <https://doi.org/10.5194/acp-7-2233-2007>.
 621
- 622 Finlayson-Pitts, B.J., Pitts, J.N. Jr. 1977. The chemical basis of air quality: Kinetics and mechanism
 623 of photochemical air pollution and application to control strategies. In *Advances in Environmental*
 624 *Science and Technology*. (7), 75-162, J.N. Pitts, Jr. and R.L. Metcalf, eds., New York, Wiley-
 625 Interscience Publication.
 626
- 627 Greene, C.J., Burleson, S.L., Crosby, J.C., Heimann, M.A., Pigott, D.C., 2020. Coronavirus disease
 628 2019: International public health considerations. *Journal of the American College of Emergency*
 629 *Physicians*. 1, 2. <https://doi.org/10.1002/emp2.12040>.
 630
- 631 Haagen-Smit, A.J., Bradley, C. E., Fox, M. M. 1956. Ozone formation in photochemical oxidation
 632 of organic substances, *Ind. Eng. Chem.* 48(9), 1484–1487. <https://doi.org/10.1021/ie51400a033>
 633
- 634 Ho, W.C., Hartley, W. R., Myers, L., Lin, M. H., Lin, Y. S., Lien, C.H., Lin, R. S. 2007. Air
 635 pollution, weather, and associated risk factors related to asthma prevalence and attack rate. *Environ.*
 636 *Res.* 104(3), 402–409. <https://doi.org/10.1016/j.envres.2007.01.007>
 637
- 638 INEC (Instituto Nacional de Estadística y Censos), 2017. Proyecciones referenciales de población a
 639 nivel cantonal-provincial. URL. <https://sni.gob.ec/proyecciones-y-estudios-demograficos>. Accessed
 640 date: 25 May 2020.
 641

- Jaeglé, L., Jacob, D.J., Brune, W.H., Wennberg, P.O. 2001. Chemistry of HO_x radicals in the upper troposphere. *Atmos. Environ.*, 35(3), 469-489. [https://doi.org/10.1016/S1352-2310\(00\)00376-9](https://doi.org/10.1016/S1352-2310(00)00376-9)
- Jaimes-Palomera, M., Retama, A., Elias-Castro, G., Neria-Hernández, A., Rivera-Hernández, O., Velasco, E. 2016. Non-methane hydrocarbons in the atmosphere of Mexico City: Results of the 2012 ozone-season campaign. *Atmos. Environ.*, 132, 258-275. <https://doi.org/10.1016/j.atmosenv.2016.02.047>
- Jenkin, M., Saunders, S.M., Pilling, M.J. 1997. The tropospheric degradation of volatile organic compounds: a protocol for mechanism development. *Atmos. Environ.*, 31(1), 81-104. [https://doi.org/10.1016/S1352-2310\(96\)00105-7](https://doi.org/10.1016/S1352-2310(96)00105-7)
- Kleinman, L.I., Daum, P.H., Lee, Y.N., Nunnermacker, L.J., Springston, S.R., Weinstein-Lloyd, J., Rudolph, J. 2001. Sensitivity of ozone production rate to ozone precursors. *Geophys. Res. Lett.*, 28(15), 2903-2906. <https://doi.org/10.1029/2000GL012597>
- Kleinman, L.I. 2005. The dependence of tropospheric ozone production rate on ozone precursors, *Atmos. Environ.* 39(3), 575–586. <https://doi.org/10.1016/j.atmosenv.2004.08.047>
- Levi, H. 1971. Normal atmosphere: Large radical and formaldehyde concentrations predicted. *Science*. 173, 141-143. <https://doi.org/10.1126/science.173.3992.141>
- Li, G., Bei, N., Tie, X., Molina, L.T., 2011. Aerosol effects on the photochemistry in Mexico City during MCMA-2006/MILAGRO campaign. *Atmos. Chem. Phys.* 11, 5169–5182. <https://doi.org/10.5194/acp-11-5169-2011>.
- Madden, M.C., Hogsett, W. E. 2001. A Historical Overview of the Ozone Exposure Problem. *Hum. Ecol. Risk Assess.* 7(5), 1121–1131. <https://doi.org/10.1080/20018091094880>
- NASA. 2020. Airborne Nitrogen Dioxide Plummets Over China. URL <https://earthobservatory.nasa.gov/images/146362/airborne-nitrogen-dioxide-plummets-over-china>. Accessed date: 25 May 2020.
- Nagpure, A.S, Gurjar, B.R., Kumar, P. 2011. Impact of altitude on emission rates of ozone precursors from gasoline-driven light-duty commercial vehicles. *Atmos. Environ.*, 45(7), 1413-1417. <https://doi.org/10.1016/j.atmosenv.2010.12.026>
- Quito Informa. 2020. La Calidad del aire en Quito se mantiene en niveles óptimos. URL <http://www.quitoinforma.gob.ec/2020/03/23/la-calidad-del-aire-en-quito-se-mantiene-en-niveles-optimos/>. Accessed date: 25 May 2020.
- Ren, X., van Duin, D., Cazorla, M., Chen, S., Mao, J., Zhang, L., Brune, W.H., Flynn, J.H., Grossberg, N., Lefer, B.L., Rappenglück, B., Wong, K.W., Tsai, C., Stutz, J., Dibb, J.E., Jobson, B.T., Luke W.T., Kelley, P. 2013. Atmospheric oxidation chemistry and ozone production: Results from SHARP 2009 in Houston, Texas. *Geophys. Res: Atmos.* 118(11), 5770-5780. <https://doi.org/10.1002/jgrd.50342>
- Saunders, S.M., Jenkin, M.E., Derwent, R.G., Pilling, M.J. 2003. Protocol for the development of the Master Chemical Mechanism, MCM v3 (Part A): tropospheric degradation of non-aromatic

- 691 volatile organic compounds. *Atmos. Chem. Phys.*, 3, 161-180. <https://doi.org/10.5194/acp-3-161->
692 2003
- 693
- 694 Secretaría de Ambiente, 2018. Informe de la Calidad del Aire del Distrito Metropolitano Quito
695 2017. URL. <http://www.quitoambiente.gob.ec/ambiente/index.php/informes#informe-calidad-del->
696 aire-2017. Accessed date: 1 Apr 2020.
- 697
- 698 Secretaría de Ambiente. 2020. Datos Horarios Históricos Red Monitoreo Aire. URL.
699 <http://www.quitoambiente.gob.ec/ambiente/index.php/datos-horarios-historicos#monoxido->
700 carbono-co. Accessed date: 1 Apr 2020.
- 701
- 702 Seinfeld, J.H., Pandis, S.N. 2006. Atmospheric chemistry and physics: from air pollution to climate
703 change. Hoboken. John Wiley & Sons, Inc.
- 704
- 705 Servicio Nacional de Gestión de Riesgos y Emergencias. 2020. Informes de Situación e Infografías
706 – COVID 19 – desde el 29 de Febrero del 2020. URL
707 <https://www.gestionderiesgos.gob.ec/informes-de-situacion-covid-19-desde-el-13-de-marzo-del->
708 2020/. Accessed date: 25 May 2020.
- 709
- 710 Shirley, T.R., Brune, W.H., Ren, X., Mao, J., Leshner, R., Cardenas, B., Volkamer, R., Molina, L.T.,
711 Molina, M.J., Lamb, B., Velasco, E., Jobson, T., Alexander, M. 2006. Atmospheric oxidation in the
712 Mexico City Metropolitan Area (MCMA) during April 2003. *Atmos. Chem. Phys.* 6, 2753–2765.
713 <https://doi.org/10.5194/acp-6-2753-2006>
- 714
- 715 Sillman, S. 1995. The use of NO_y, H₂O₂, and HNO₃ as indicators for ozone □ NO_x □ hydrocarbon
716 sensitivity in urban locations. *J. Geophys. Res. - Atmos.*, 100(D7), 14175-14188.
717 <https://doi.org/10.1029/94JD02953>.
- 718
- 719 Thornton, J.A., Wooldridge, P.J., Cohen, R.C., Martinez, M., Harder, H., Brune, W.H., Williams,
720 E.J., Roberts, J.M., Fehsenfeld, F.C, Hall, S.R, Shetter, R.E., Wert, B.P., Fried, A. 2002. Ozone
721 production rates as a function of NO_x abundances and HO_x production rates in the Nashville urban
722 plume. *J. Geophys. Res. - Atmos.* 107(D12). <https://doi.org/10.1029/2001JD000932>
- 723
- 724 Trebs, I., Bohn, B., Ammann, C., Rummel, U., Blumthaler, M., Königstedt, R., Meixner, F.X., Fan,
725 S., and Andreae, M. O., 2009. Relationship between the NO₂ photolysis frequency and the solar
726 global irradiance. *Atmos. Meas. Tech.* 2, 725–739. <https://doi.org/10.5194/amt-2-725-2009>.
- 727
- 728 Wolfe, G.M., Marvin, M.R., Roberts, S.J., Travis, K.R., Liao, J. 2016. The Framework for 0-D
729 Atmospheric Modeling (F0AM) v3.1. *Geosci. Model Dev.*, 9, 3309–3319.
730 <https://doi.org/10.5194/gmd-9-3309-2016>.
- 731
- 732 Wolfe, G., 2020. Overview of the Framework for 0-D Atmospheric Modeling (F0AM). URL.
733 https://github.com/AirChem/F0AM/blob/master/F0AM_UserManual.pdf. Accessed date: 7 August
734 2020.
- 735
- 736
- 737
- 738



Fig. 1. a) Location the Atmospheric Measurement Station (EMA, Spanish acronym) at USFQ relative to Quito (red balloon). Blue dots mark locations of three stations managed by Quito's air quality network (Cotocollao, Belisario and Los Chillos), whose CO data were averaged. b) Quito location relative to Ecuador. Maps were extracted from Google Earth.

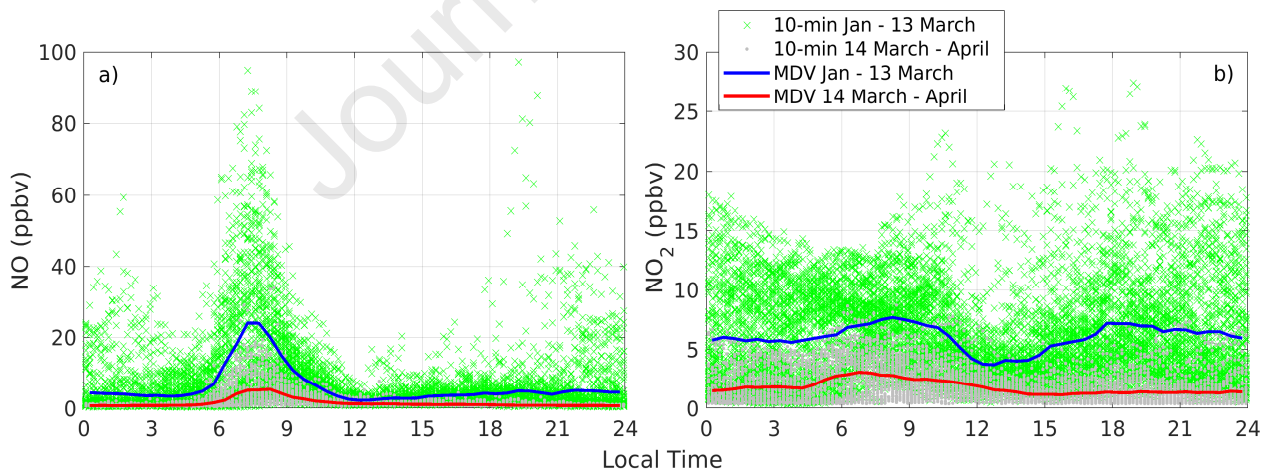


Fig. 2. a) NO measured at EMA USFQ before (green crosses and blue line) and after (gray dots and red line) the COVID-19 lockdown. b) The same, but for NO₂. Crosses and dots are 10-minute data and lines are median diurnal variations (MDV). Dates before and after the lockdown were Jan-13 March and 14 March-April, respectively.

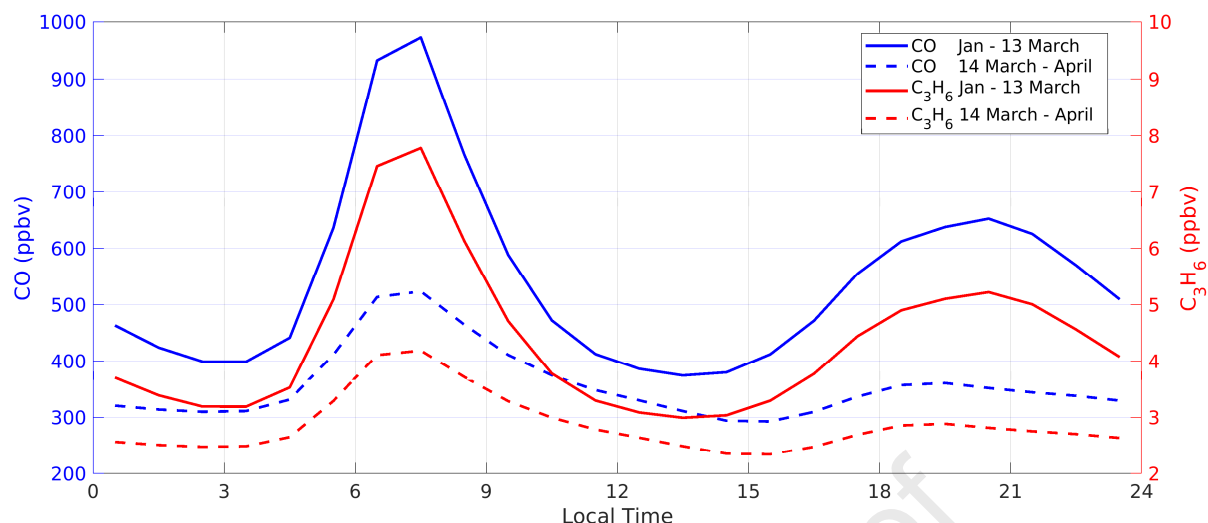


Fig. 3. Mean diurnal variation of CO (blue) and C_3H_6 (propene, red) before (solid lines) and after (dashed lines) the COVID-19 lockdown (Jan-13 March and 14 March-April, respectively). CO is the average from three City stations. Propene was derived by scaling CO (for other VOCs see Appendix S3).

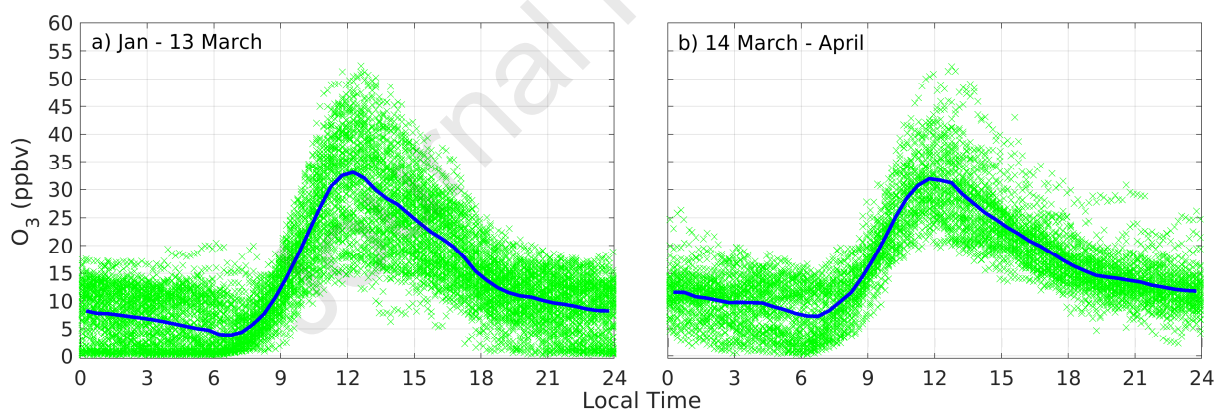


Fig. 4. Ozone measured at EMA USFQ a) before and b) after the COVID-19 lockdown (Jan-13 March and 14 March-April, respectively). Crosses are 10-minute data and solid lines are MDVs.

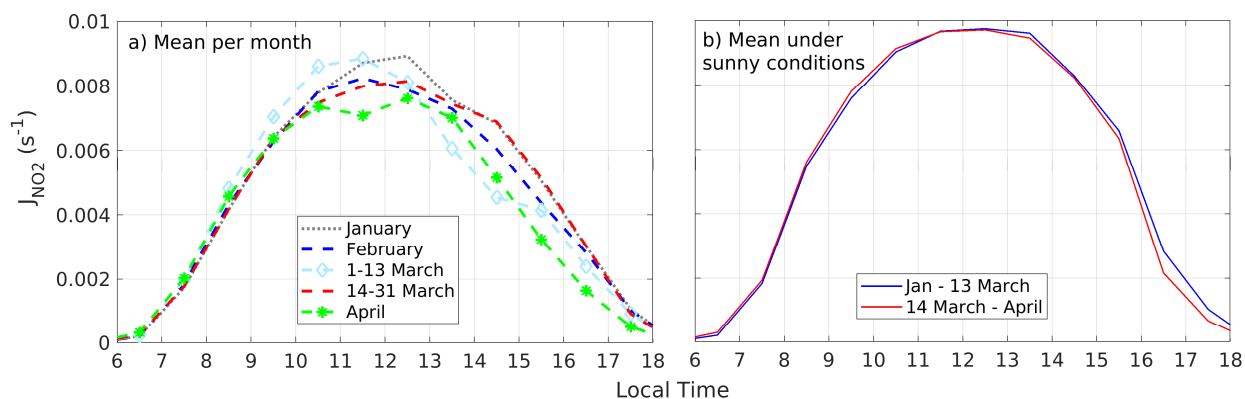


Fig. 5. a) J_{NO_2} mean diurnal variation for January (dotted gray), February (dashed blue), 1-13 March (light blue and diamonds), 14-31 March (dashed red), and April (dashed green and stars). **b)** Mean J_{NO_2} under sunny conditions before (Jan-13 March, blue line) and after (14 March-April, red line) the COVID-19 lockdown.

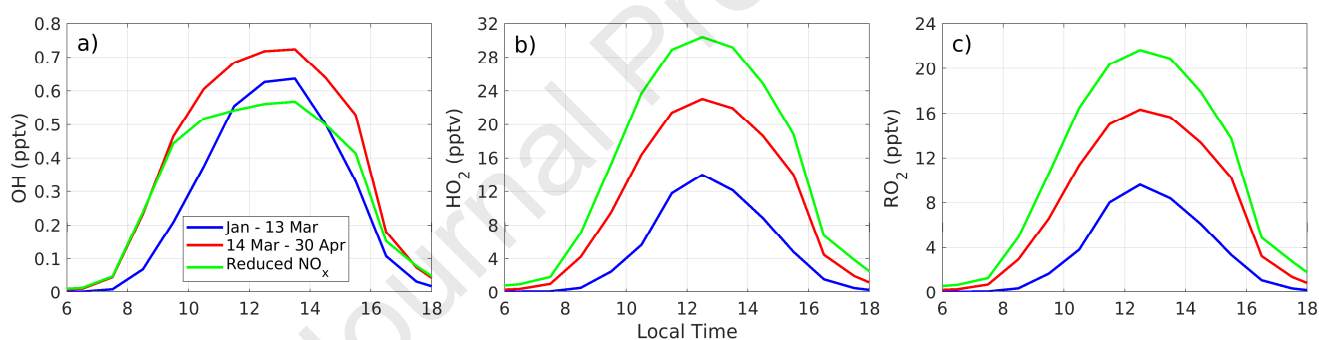
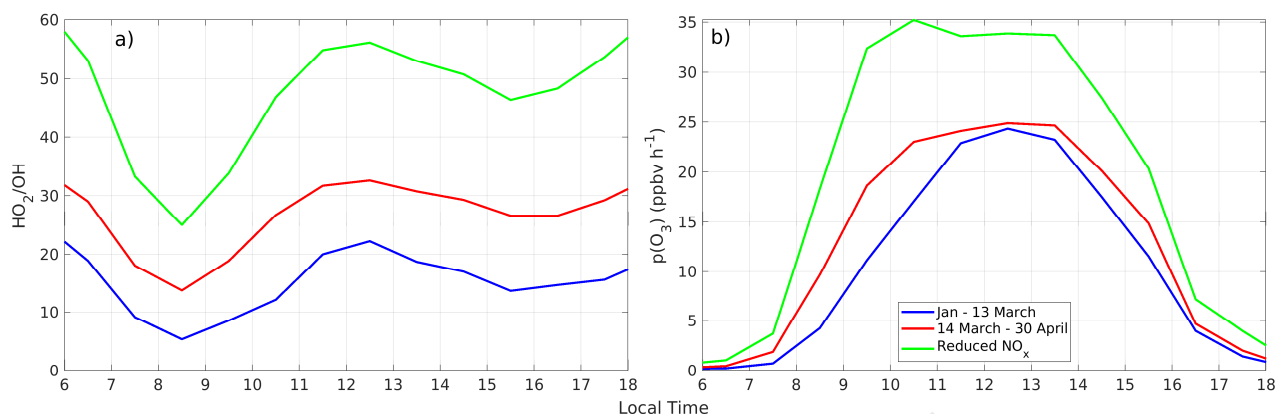


Fig. 6. Mean diurnal variations for **a)** OH, **b)** HO₂, and **c)** RO₂ before (January-13 March, blue line) and after (14 March -April, red line) the COVID-19 lockdown. The green line corresponds to the reduced-NO_x simulation with post-lockdown NO_x levels and pre-lockdown VOCs.

833



834

835 **Fig. 7. a)** HO_2/OH ratio and **b)** $p(\text{O}_3)$ before and after the lockdown. The blue line is the mean
 836 diurnal variation for each quantity for January - 13 March (pre-lockdown), red corresponds to 14
 837 March - April (post-lockdown), and the green line is the test simulation with reduced- NO_x (post-
 838 lockdown levels) and pre-lockdown VOCs.

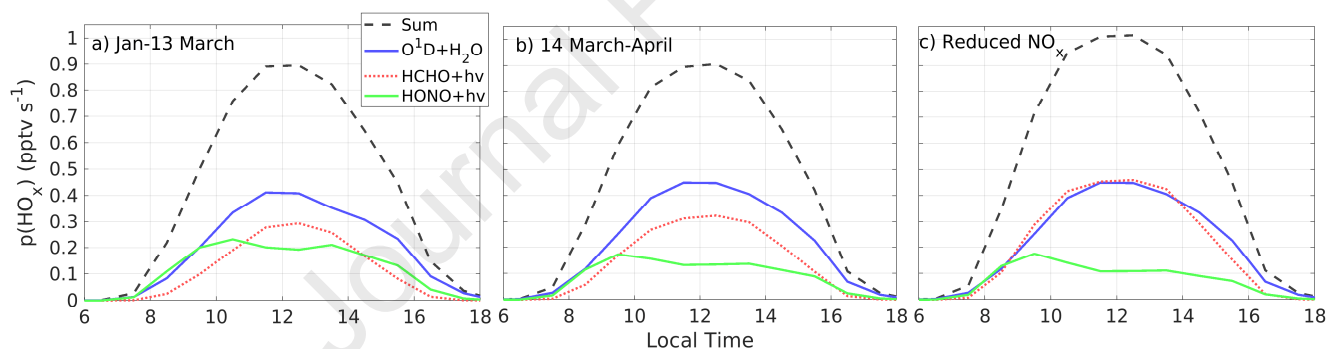
839

840

841

842

843



844

845

846 **Fig. 8.** Total radical production, $p(\text{HO}_x)$, (black dashed line) and individual contributions by
 847 photolysis of ozone followed by the reaction of O^1D with water vapor (blue line), formaldehyde
 848 photolysis (red dotted line), and HONO photolysis (green line) for a) January-13 March (pre-
 849 lockdown), b) 14 March -April (post-lockdown), and c) Test simulation with reduced- NO_x (post-
 850 lockdown levels) and pre-lockdown VOCs levels.

851

852

853

854

855

856

857

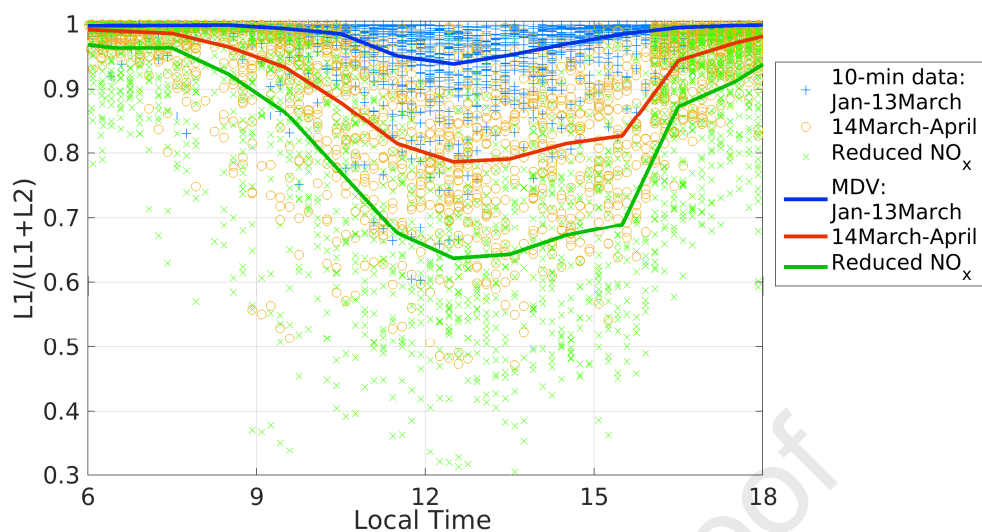
858

859

860

861

862



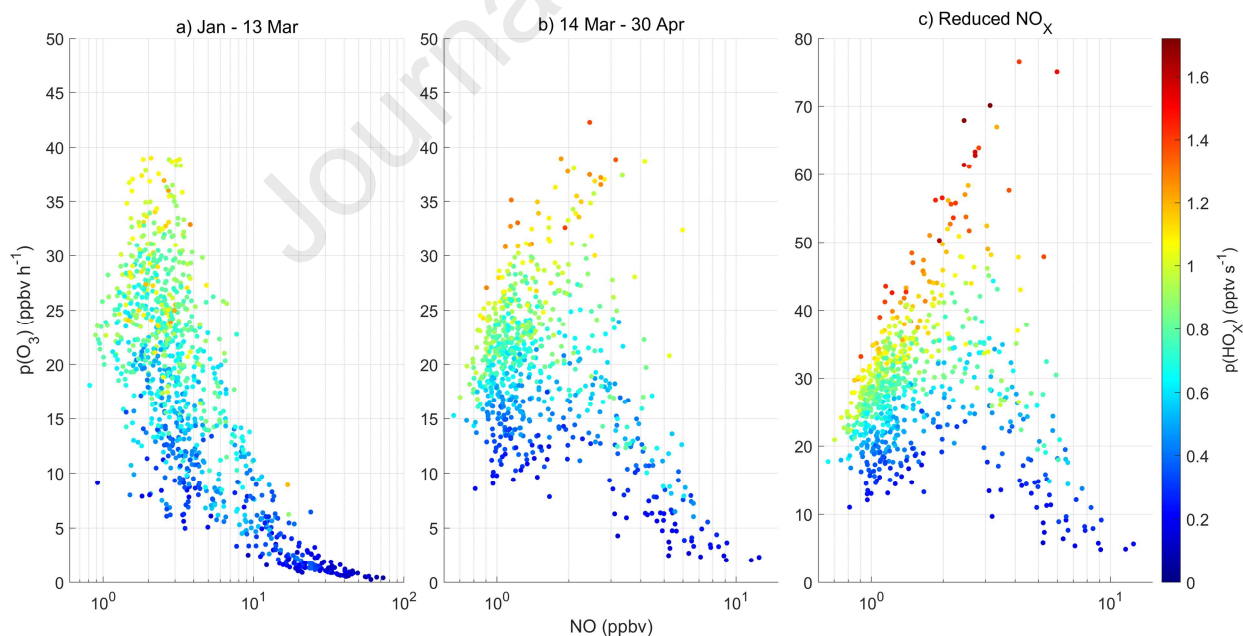
878

879

880 **Fig. 9.** Ratio of radical losses to nitric acid (L1) to total losses (L1+L2), where L2 is the loss to
 881 hydrogen peroxide. 10-minute data are represented by blue crosses (January to 13 March, pre-
 882 lockdown), orange circles (14 March-April, post-lockdown), and green crosses (simulation with
 883 reduced-NO_x at post-lockdown levels and pre-lockdown VOCs). Solid lines (blue, red, and green)
 884 are corresponding mean diurnal variations for each case.

885

886



887

888 **Fig. 10.** Ozone production rates, $p(\text{O}_3)$ (10-minute data), in NO space sorted by magnitudes of
 889 $p(\text{HO}_x)$ for: **a)** January to 13 March (pre-lockdown); **b)** 14 March to April (post-lockdown), and **c)**
 890 Reduced-NO_x simulation with post-lockdown NO_x and pre-lockdown VOCs.

Highlights

- NO_x levels dropped by a factor of five after mobility restrictions.
- The chemical regime of ozone production shifted from NO_x-saturated to NO_x-limited.
- Ozone production rates increased in the mid-morning after mobility restrictions.

Declaration of interests

☒ The authors declare that they have no known competing financial interests or personal relationships that could have appeared to influence the work reported in this paper.

☐ The authors declare the following financial interests/personal relationships which may be considered as potential competing interests: